Biophysical Chemistry 142 (2009) 76–83

Contents lists available at ScienceDirect

Biophysical Chemistry

journal homepage: http://www.elsevier.com/locate/biophyschem

Conformation and dynamics of DNA molecules during photoreversible condensation

Anne-Laure M. Le Ny, C. Ted Lee Jr. *

Department of Chemical Engineering and Materials Science, University of Southern California, Los Angeles, CA 90089-1211, USA

ARTICLE INFO

Article history:
Received 11 September 2008
Received in revised form 4 March 2009
Accepted 8 March 2009
Available online 31 March 2009

Keywords:
DNA compaction and expansion kinetics
Photoresponsive surfactants

ABSTRACT

Direct observation of the mechanism and dynamics of photo-initiated DNA compaction and re-expansion using a light-responsive cationic surfactant has been achieved with fluorescence microscopy. The surfactant undergoes a reversible photoisomerization upon exposure to visible (*trans* isomer, relatively hydrophobic) or UV (*cis* isomer, relatively hydrophilic) light. Thus, surfactant binding to DNA and the DNA condensation that result can both be initiated and controlled with light illumination. The inherent kinetics of DNA conformational changes, directly visualized following the *in situ* light "trigger" of surfactant photoisomerization, are found to occur at rates of approximately 9 μm/s or 240 kbp/s, at or near rates that can be achieved in natural processes. Furthermore, observation of photo-initiated DNA compaction, free of the effects of shear or mixing, provides evidence of a condensation mechanism that nucleates at the ends of the macromolecule. Ethidium bromide displacement studies, employed to gain insight on the mode of interaction between the photo-surfactant and DNA, also reveal the importance of both electrostatic and hydrophobic forces in surfactant binding and DNA condensation.

1. Introduction

DNA compaction is an important biological process by which DNA is reversibly packed, stored, and protected in living organisms. This occurs *in vivo* through the interaction of DNA with low molecular weight compounds such as spermine or spermidine for compaction inside virus heads [1], or with higher molecular weight compounds such as histones for packaging of genetic material into chromosomes. Compaction of DNA has also been shown to be induced *in vitro* by complexation of nucleic acids with cationic surfactants [2–6], lipids [7,8], multivalent ions [9–12], and alcohols [13,14]. Neutralization of the repulsive negative charges responsible for the elongated-coil conformation of DNA can induce compaction into a tight, globular structure [11] with sizes typically ranging from 50–200 nm largely independent of DNA molecular weight, as measured by TEM [15,16]. However, the process of DNA compaction, although attracting a great deal of interest, is still not completely understood.

In non-viral gene therapy applications, DNA condensation has been shown to be essential to protect DNA from nuclease [11], and to allow entry of DNA into cells, mainly by the endocytic pathway [17]. However, while the complexing agents mentioned above can increase *cellular uptake* as a result of DNA neutralization and compaction, the tight binding of these same agents to DNA may also generally preclude or greatly reduce the interaction of DNA with intracellular molecules such as importin or transportin and the subsequent *nuclear uptake* [18,19], reducing transfection efficiencies relative to viral delivery methods. Indeed, it has been shown that vector unpacking can be a limiting barrier to gene delivery [20,21]. Thus, the development of photoreversible DNA complexes could provide a triggered release of DNA from the carrier and potentially increase transfection efficiencies, while at the same time providing a convenient method to investigate the mechanistic detail of DNA compaction.

Traditionally, to trigger DNA release from a carrier complex and, therefore, induce DNA re-expansion requires a change of the thermodynamic properties of the solvent such as changes in pH [22], ionic strength [23], or complexing agent concentration through dilution [24]. Recently, a method to reversibly photo-control DNA conformation has been developed using light-responsive cationic surfactants as the complexing agent [2]. Through measurements of the ensemble-averaged hydrodynamic radius of DNA-photosurfactant complexes, the relatively-hydrophobic *trans* isomer of the surfactant, predominant under visible light illumination, was found to be more effective at binding to DNA and inducing DNA condensation than the relatively-hydrophilic *cis* form obtained under UV illumination. Similar control of DNA conformation using redox-active surfactants has also recently been achieved by Abbott *et al.* using electrochemical methods [25]. In this work, fluorescence microscopy is used to directly visualize conformational changes of individual T4-DNA molecules in solution triggered solely with light illumination, permitting evaluation of both the mechanism and kinetics of the light-initiated transitions. Although the theory of the kinetics of polymer collapse has been investigated through simulations [26–28], few experimental studies

* Corresponding author. Mork Family Department of Chemical Engineering and Materials Science, University of Southern California, 925 Bloom Walk, HED 207, Los Angeles, CA 90089-1211, USA. Tel.: +1 213 740 2066; fax: +1 213 740 8053.
E-mail address: tedlee@usc.edu (C.T. Lee).

0301-4622/$ – see front matter © 2009 Elsevier B.V. All rights reserved.
doi:10.1016/j.bpc.2009.03.010

have been able to capture this phenomenon and measure the kinetics of DNA coil-to-globule transitions free of potential experimental artifacts due to elongational flow or mixing. Fluorescence spectroscopy is further used to perform ethidium bromide displacement experiments in order to investigate the binding affinity of the light-responsive surfactant to DNA and the molecular mechanisms responsible for compaction.

2. Materials and methods

2.1. Materials

An azobenzene trimethylammonium bromide surfactant (azoTAB) of the forms described in Scheme 1 similar to those used in previous studies to photo-control DNA compaction [2] and protein folding [29–31], was synthesized according to published procedures [32] via an azo coupling reaction of 4-ethlyalaniline with phenol subsequently followed by reactions with 1,4-dibromobutane and finally trimethylamine. Surfactant purity was 99% determined by GC and NMR. This particular surfactant was chosen after testing several similar azobenzene-based photosurfactants with varying lengths of the two hydrocarbon spacers. Screening tests where performed through phase behavior measurements, since DNA precipitation would require surfactant binding to and neutralizing of DNA (both also necessary for DNA compaction). The current surfactant was chosen based on having the highest difference in surfactant concentration required for precipitation under visible versus UV light.

The surfactant undergoes a reversible photoisomerization when exposed to UV (*trans*→*cis*, $\lambda_{max}^{trans}=350$ nm) or visible (*cis*→*trans*, $\lambda_{max}^{cis}=434$ nm) light. When placed in the dark, the surfactant will adopt the more stable, *trans* isomer in about 24 h. Conversion to the *cis* form during the microscopic experiments was achieved through illumination of the samples with a 200-W Mercury arc lamp (Oriel, model no. 6283) equipped with a liquid light guide (Oriel, model no. 77557), a fiber-bundle focusing assembly (Oriel, model no. 77800) and a 320-nm band pass filter (Oriel, model no. 59800). A heat-absorbing filter (Oriel, model no. 59060) was placed in the beam path to absorb IR light produced by the lamp. These combined filters effectively isolate the 365-nm line (UV–A) of the mercury lamp. Exposure of DNA samples to this light source did not result in strand separation or cleavage, checked during visual observation as well as absorbance measurements (e.g., DNA unraveling from a double-stranded to a single-stranded molecule results in a large [~30%] absorption change, while DNA cleavage can be readily detected during fluorescence microscopy experiments) [2]. Conversion back to the *trans* form was achieved through illumination as above using a 435.8-nm band pass filter (Oriel, model no. 56551). In the case of experiments where the surfactant was converted to the *cis* form prior to being mixed with DNA, conversion was achieved through exposing a stock surfactant solution to an 84-W long wave UV lamp-365 nm (Spectroline, model no. XX-15A) for at least 1 h.

2.2. Fluorescence microscopy

T4-phage DNA (165.6 kbp, 1.076×10^8 Da), was purchased from Wako Chemical (cat. no. 318-03971) and visualized with the fluorescent dye YOYO-3® ($\lambda^{ex}/\lambda^{em}=612/631$ nm) from Molecular Probes (cat. no. Y3606). Samples were observed with an Olympus IX71 inverted fluorescence microscope equipped with a 100× oil-immersed objective lens (UPlanFl, N.A. = 1.3) and a U-N41027 CAL CRIM C-58158 filter cube as described below. Images were recorded with a Hamamatsu digital CCD camera (model no. C4742-95) at a frame rate of 16.3 Hz. A band-pass filter (Chroma, HQ645/75m) letting pass wavelengths from 600–680 nm was placed in front of the camera to prevent light from the mercury arc lamp leaking through the microscope optics from saturating the camera. To reduce potential light-induced damage of DNA molecules, a 20% neutral density filter was placed in front of the excitation source. Under these conditions, no strand breakage and only minimal photobleaching of the dye was observed during the course of the experiments (~20 s). Hence, it was not necessary to add a free radical scavenger (e.g., β-mercaptoethanol), facilitating the study of DNA-surfactant interactions with a minimal number of components.

The concentrated DNA solution was diluted to 0.6 μM (base pair) in TE buffer (10 mM Tris, 1 mM EDTA) and gently mixed with the dye solution to a ratio of 20 base pairs per dye molecule. The DNA solution was then placed in a custom-made slide consisting of the top part of a disposable polymethylmethacrylate UV-vis cuvette glued to a microscope cover slip, providing a $(1\times1\times1)$ cm^3 receptacle for the sample. Approximately 250 μL of DNA-dye solution was placed in this cell and kept open to air. This custom-made slide, only used once per sample, was necessary to allow visualization of DNA complexes at distances of up to 50 μm from the cover slip, as it was observed that compacted DNA was strongly attracted to glass surfaces. Moreover, this setup allowed for measurements of the kinetics of compaction following direct addition of 10 μL of a 1.25 mM surfactant stock solution to a pure DNA solution. In this manner, DNA compaction could be readily observed adjacent to the location of surfactant addition, with the rapid diffusion of surfactant molecules from the concentrated drop region resulting in local surfactant concentrations sufficient to condense the DNA molecule.

A DNA solution was first placed in the receptacle and complexes of DNA and azoTAB surfactant were formed by addition of a concentrated stock solution of surfactant in TE buffer, with the concentration of the stock solution determined with UV–visible spectroscopy from the extinction coefficient of 22,400 L mol^{-1} cm^{-1} at 350 nm [33]. The final solution containing DNA and surfactant was gently swirled before observation and a video of the resulting solution was taken under both visible and, after a 2 min exposition through a fiber optic, UV light. This operation was repeated for successively higher surfactant-to-DNA base pair ratios (*r*-ratios), resulting in a modest dilution of ~10% in the DNA concentration, accounted for in the calculation of the *r*-ratio. To access higher *r*-ratios and avoid DNA precipitation at elevated *trans*-azoTAB concentrations, the surfactant stock solution was pre-converted to the *cis* form through UV illumination prior to

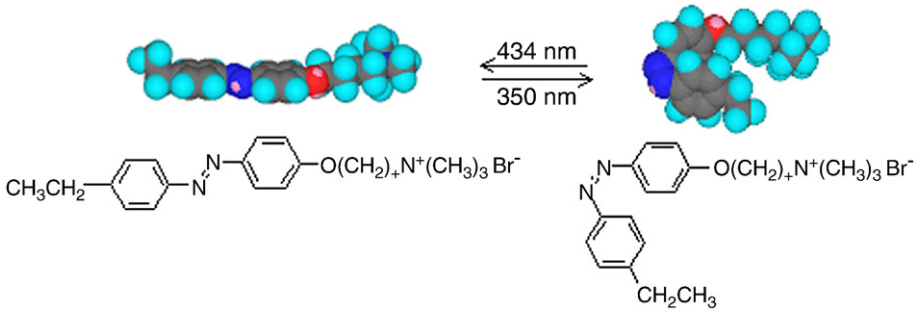

Scheme 1. Photoisomerization of the azoTAB surfactant.

addition into the DNA solution. While it is true smaller precipitates would not be seen by the eye, since the majority of the experiments were performed using fluorescence microscopy, such small aggregates would be easily detected (and in some cases were observed at elevated surfactant concentrations). Thus, all experiments were conducted in regions free of aggregation (both local and macroscopic).

Images of ~200 DNA molecules from randomly selected video frames were used at each *r*-ratio and light condition for subsequent data analysis. The length of each DNA molecule was then calculated by processing the DNA image using the Matlab command *MajorAxisLength*, which returned the length in pixels of the major axis of an ellipse with the same normalized second central moment as the observed image. The pixel length was converted to the actually length in micrometers using a calibration standard. This automated procedure was manually checked using a smaller sample set to ensure reliability. For the time-based experiments, a 500-W mercury bulb was employed to overcome any surfactant conversion that would be caused by the excitation source of the microscope. Switching between UV and visible light occurred within one video frame and was performed with a manual shutter. A change in background intensity when light is turned on was easily detected thus, time $t=0$ was taken as the first frame where this intensity change was detected.

2.3. UV–vis spectroscopy

Surfactant photoisomerization kinetic measurements were performed on an Agilent model 8453 spectrophotometer using a 0.1 mm path length quartz cuvette to mimic the focal distance of the UPlanFl objective lens. A liquid light guide was used to illuminate a 700-μM surfactant solution in water while time-resolved absorption measurements were taken. Due to the resolution of the spectrophotometer (0.5 s) and the time required to open the manual shutter (~0.1 s), the rates from several cycles were averaged as opposed to arbitrarily assigning an initial time.

2.4. Fluorescence spectroscopy

Fluorescence emission measurements of ethidium bromide (Fluka) were performed on a QuantaMaster spectrofluorometer (Photon Technology International, model QM-4) at 25 °C using a 1-cm path length cuvette. The probe was excited at 535 nm and the emission was recorded at 595 nm with excitation and emission slit widths of 4 nm. Herring testes DNA, type XIV, containing 6.2% sodium salt (Sigma, D-6898), with a polydisperse molecular weight covering a broad range below 1500 bp as determined by gel electrophoresis, was dissolved in TE buffer overnight and the concentration was measured spectroscopically using an extinction coefficient of 6600 M^{-1} cm^{-1} at 260 nm. The solution of DNA complexed with ethidium bromide was prepared by adding the desired amount of DNA and ethidium bromide stock solutions at a ratio of 2 base pairs per dye molecule. The final base-pair concentration of herring testes DNA was 0.6 μM, identical to the concentration of T4 DNA used in the microscope experiments. DNA-surfactant complexes were then formed by successive addition of a concentrated stock surfactant solution, and a spectrum was recorded at each condition with the solution continuously stirred. Complexes between DNA and the *cis*-azoTAB surfactant were formed by first converting the stock surfactant solution to the *cis* state using the long wave UV lamp. The surfactant isomeric state was confirmed at the end of the experiment with UV–vis spectroscopy.

3. Results and discussion

3.1. Direct detection of DNA compaction

Values of the T4-DNA average end-to-end distance determined from fluorescence microscopy as a function of the surfactant-to-DNA base pair ratio, *r*, are shown in Fig. 1. At low azoTAB concentrations ($r<160$, or [azoTAB]<100 μM), DNA molecules remain in the elongated-coil state with an average length of ~4 μm, similar to literature values for uncompacted T4-DNA [3,34]. Increasing the *r*-ratio above 160 under visible light, however, causes a significant proportion of the DNA molecules to become compacted as seen in the photomicrographs, resulting in a decrease in the average length. Since the compaction process is well-known to be a discrete phenomenon (i.e., at equilibrium a DNA molecule may only be elongated or compact, with no partial condensation observed [3], consistent with the images in Fig. 1), the reported values represent the average over these two conformational states. Further increasing the surfactant concentration under visible light beyond an *r*-ratio of ~240 then results in complete condensation of all DNA molecules into the compacted state with an average diameter of ~1.1 μm, similar to values reported for compacted T4-DNA [13,35]. Note that the values in Fig. 1 are naturally influenced by the "blurring effect" due to the optical diffraction limit, which is in the order of 0.3 μm [3].

Under UV-light with azoTAB in the relatively hydrophilic *cis* conformation, DNA condensation is delayed until significantly higher surfactant concentration, as shown in Fig. 1. The onset of compaction is not observed until $r\sim650$, while DNA is not fully compacted until $r\sim950$. Note that at these *r*-ratios there is no visible-light data as precipitation of compacted DNA on the cover slip prevented imaging. Comparing the data taken under different light conditions it can be seen that about 3–4 times higher *cis*-azoTAB concentration is required to induce a similar effect on DNA as the *trans* surfactant, consistent with the previous light-scattering study [2]. The fact that both the visible (*trans*) and UV (*cis*) forms of azoTAB are capable of compacting DNA suggests that the isomers have similar modes of action and argues against azoTAB intercalation between base pairs, which generally requires planar ligands. Thus, the possibility that the *cis*, bent form of the surfactant may become intercalated is believed to be quite low. In addition, previous measurements with the dye crystal violet have demonstrated significant π–π stacking interactions between adjacent surfactant molecules in the condensed DNA complex [2], suggesting a surface-binding mechanism.

To provide more detail into the compaction process, the distributions of measured DNA long-axis dimensions as a function of *r*-ratio and light illumination are shown in Fig. 2. With DNA in the elongated-coil conformation, the distributions are fairly broad as expected, with

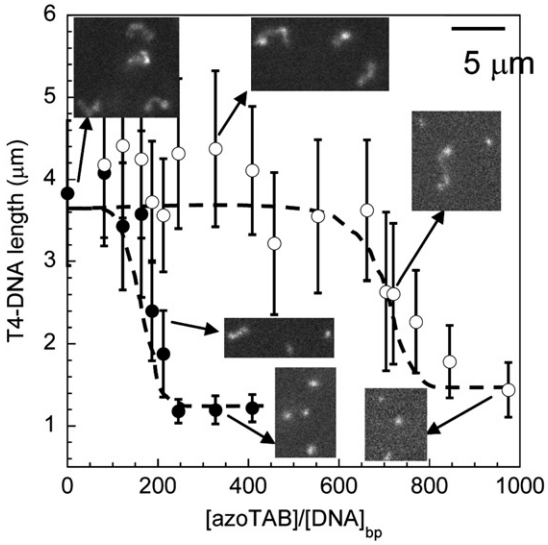

Fig. 1. Average long-axis length of T4-DNA as a function of the surfactant-to-DNA base pair ratio (*r*) measured under visible (●) and UV light (○). [T4-DNA] = 0.55–0.6 μM, [YOYO-3] ~ 0.03 μM. Error bars represent the standard deviation (see also Fig. 2). Representative fluorescent microscope images are also displayed.

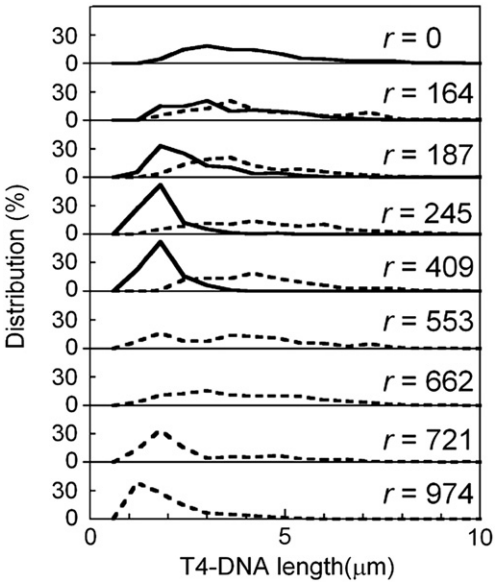

Fig. 2. Relative distribution of the long-axis lengths of T4-DNA at various *r*-ratios, measured under visible (-) and UV light (--). Areas of the histograms have been normalized.

DNA lengths ranging from 2–8 μm. Due to rotational diffusion, however, the measured end-to-end distances are projections in the focal plane as DNA molecules may be tilted out-of-plane when observed. Thus, the large spread in sizes observed in Fig. 2 is not entirely a result of DNA macromolecular flexibility. Condensation of a fraction of the DNA molecules is again observed at $r \sim 160$ under visible light and $r \sim 700$ under UV light, with full condensation occurring at *r*-ratios of about 200 and 800, respectively.

As Fig. 1 indicates, by using azoTAB to condense DNA, complete photoreversible control of DNA conformation with simple light illumination can be obtained. Thus, the *kinetics* of DNA conformational changes can be measured in a relatively simple and unobtrusive manner, as seen in Fig. 3. At $r = 257$ under UV light, DNA is in the elongated-coil state, as expected from Fig. 1. Illuminating this DNA-surfactant solution with visible light results in DNA compaction within *ca.* 0.36 s, as shown by the sequence of images in Fig. 3. Subsequent UV-illumination causes DNA molecules to re-expand within *ca.* 0.8 s. It was observed that repeated cycles of photoreversible control of DNA conformation in this manner could be induced virtually indefinitely, provided that the dye does not photobleach (total observation time is ~20 s). For comparison, several trajectories of individual DNA molecules undergoing light-initiated compaction and expansion are shown in the graphs in Fig. 3, while the solid line shows the time course of the average end-to-end distance for all observed molecules. The broad range of pathways that the molecules seem to follow is due to the fact that the molecules are undergoing tumbling motions and diffusion in and out of the plane of focus, which further prevent measurements for periods of time much longer than ~1 s The kinetics of compaction and expansion are both found to range from 0.4 to 0.8 s, while the average time for each is about 0.7 s for both conformational rearrangements.

To estimate the rates of these conformational changes, the measured DNA end-to-end distances, which as mentioned previously are projections in the focal plane, must first be equated to the true macromolecular sizes. This can be done by averaging the projected length, $l \cos\theta$, over all angles θ relative to the focal plane, which gives an average projected length of $2/\theta$ times the true macromolecular length, *l*. Thus, using the averaged projected length of uncompacted DNA of 4 μm from Fig. 1 (where 200 molecules are averaged, as opposed to Fig. 3) gives a true average length of T4-DNA of 6.3 μm. This equates to light-induced compaction and expansion rates of ~9 μm/s or ~240 kbp/s in Fig. 3.

Previous studies have attempted to mimic natural DNA conformational changes in order to evaluate the kinetics of these processes. Protamine, a protein responsible for inducing DNA compaction in spermatids, was found to condense DNA at rates ranging from 1−9 μm/s or 2.4–22 kbp/s, depending on the concentration of protamine [24]. Other spermatid nuclear proteins were found to induce DNA compaction with similar rates [36]. In these studies, condensation rates were measured in a flow cell apparatus with DNA, attached at one end to a laser-trapped bead, stretched under flow. Chromatin assembly has also been investigated upon the introduction of histones by tracking the compaction of DNA, attached at one end to a microscope slide, extended under flow [37]. Condensation rates on the order of 0.01–6 μm/s or 1.9–103 kbp/s were achieved and found to be a function of the histone concentration as well as the shear rate in the flow cell [38]. Similar studies have been performed in artificial compaction systems, such as the compaction of T4-DNA, in this case free in solution, occurring at a rate of about 1 μm/s upon mixing with the cationic surfactant cetyltrimethylammonium bromide (CTAB) [3].

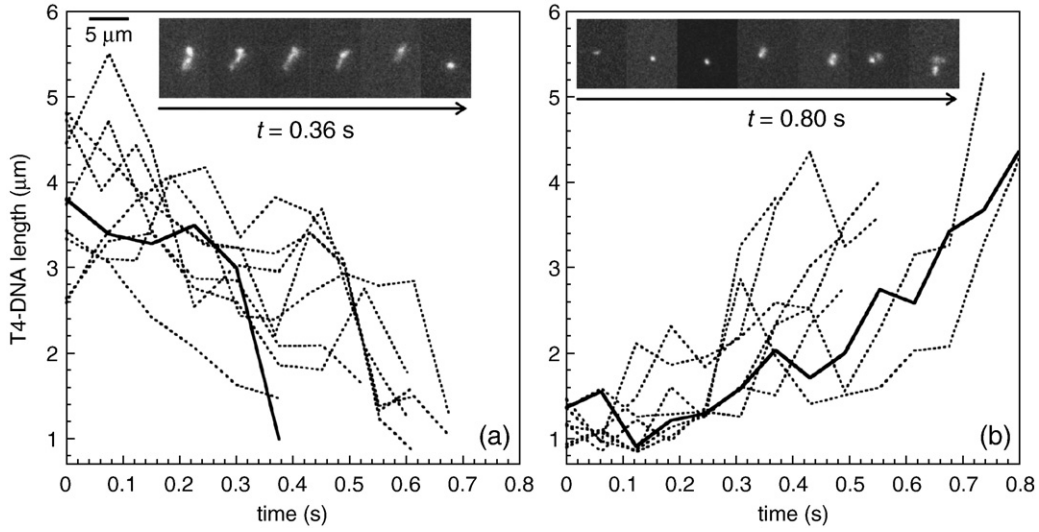

Fig. 3. Dynamics of photo-induced (a) compaction and (b) expansion of T4-DNA. The solid line represents compaction and expansion from the sequence of images shown above each graph. The surfactant-to-DNA base pair ratio is 257 in TE buffer.

In contrast, Fig. 3 allows investigation of the kinetics of DNA conformational changes induced with a simple light trigger, independent of elongational flow or mixing. The time response of this photo "switch" can be estimated by considering the individual steps required to induce a change in DNA conformation with light illumination: (1) surfactant photoisomerization, (2) association/dissociation of surfactant molecules with DNA, depending on the process, and (3) compaction or expansion of DNA. To examine step (1), measurements of photoisomerization rates were performed as shown in Fig. 4. In the displayed spectra, the *trans*-to-*cis* conversion was probed with triggered exposure to 365-nm UV light, while the surfactant was allowed to relax back to the *trans* form relatively slowly by simply switching off the 365-nm light, a natural result of exposure of the solution to a range of visible light wavelengths during the *in situ* UV–vis absorption measurements. The *trans*-to-*cis* conversion can be fit as a first-order rate process [39] according to the equation $f_{trans} = e^{-kt}$ as shown in Fig. 4b, where the fraction of surfactant remaining in the *trans* form following exposure to 365-nm UV light was defined for convenience as $f_{trans} = (A_{350} - A_{350,initial})/(A_{350,final} - A_{350,initial})$. In this manner, the rate constant for the *trans*-to-*cis* photoisomerization was found to be $k = 3.5\ s^{-1}$. A similar rate constant was obtained when the surfactant concentration was reduced by a factor of two (not shown), indicating that the process was not limited by light penetration into the sample. Furthermore, previous evidence has demonstrated that neither the photostationary state nor the photoisomerization kinetics are influenced by the presence of DNA [2].

As detailed by Shang et al. using a similar azobenzene-based surfactant ("$C_4AzoOC_2E_2$") [39], this photoisomerization rate constant would be determined by $k = \varepsilon I_0 \phi$, where ε is the molar absorption coefficient at a given wavelength of light with intensity I_0, while ϕ is the quantum efficiency for the photoisomerization process (i.e., the fraction of excited species undergoing isomerization). Thus, k_{azoTAB} can be estimated from $k_{C4AzoOC2E2}$ ($= 0.4\ s^{-1}$) [39] based on the relative absorption coefficients at 365-nm of azoTAB ($20\ mM^{-1}cm^{-1}$) [33] compared to $C_4AzoOC_2E_2$ ($5\ mM^{-1}cm^{-1}$) [39,40] along with the relative light intensities (i.e., Shang et al. used an identical optical setup except for a 200-W mercury bulb compared to the 500-W bulb in the present study). Using this approach gives a value of $k_{azoTAB} = 4.0\ s^{-1}$ assuming $\phi = 1$ (shown to be the case for $C_4AzoOC_2E_2$), in reasonable agreement with the value determined in Fig. 4b given the experimental uncertainty.

A *trans*-to-*cis* rate constant of $3.5\ s^{-1}$ equates to a photoisomerization half-life of 0.2 s, meaning that 50% of the azoTAB molecules are converted from the *trans* isomer (strong DNA interactions) to the *cis* isomer (weak DNA interactions) within this time. Thus, at the *r*-ratio of 257 employed in the DNA conformational measurements in Fig. 3, the "effective" *r*-ratio (i.e., the *r*-ratio of the remaining *trans* isomers) is reduced to ~125 within 0.2 s. As seen in Fig. 2, this effective *r*-ratio would be sufficient to induce DNA expansion, which was shown in Fig. 3b to require ~0.7 s. Interestingly, during the first 0.2 s of observation in Fig. 3b only modest degrees of DNA expansion occur in some molecules (although this is beginning to approach the resolution of the technique). This apparent "lag phase" may then correspond to the amount of time required to isomerize a sufficient amount of azoTAB (i.e., 50%) to transition from condensing to non-condensing conditions.

Attempts were made to probe this potential lag phase by increasing the *r*-ratio to 400, which would then require two-thirds of the azoTAB molecules to convert to the *cis* form to achieve an effective *r*-ratio of 125 as above. However, no significant differences in DNA expansion rates were observed (within the resolution of the technique), likely expected due to $t_{2/3}$ (0.3 s) being similar to $t_{1/2}$ (0.2 s). *R*-ratios greater than 400 could not be studied due to the aforementioned phase separation under visible light. Nevertheless, while there may be a slight lag upon photo-inducing DNA expansion, the rate of the DNA conformation transition once expansion has begun would not be expected to be limited by the rate of surfactant isomerization based on the relative rates of the two processes.

Using a similar strategy as employed above, *cis*-to-*trans* isomerization of azoTAB would be expected to occur at a rate of $0.6\ s^{-1}$ upon absorption of 435.8-nm from the 500-W mercury arc lamp, estimated from the reported value for $C_4AzoOC_2E_2$ ($= 0.083\ s^{-1}$) again with an identical optical setup [39]. However, a direct comparison of this rate of azoTAB isomerization and the resulting rate of DNA compaction is complicated by two effects. First, as previously discussed, light illumination associated with the spectroscopic measurements inherently produces *cis*-to-*trans* isomerization at a rate of $0.21\ s^{-1}$ calculated from the data in Fig. 4-inset. Thus, care must be taken to decouple the effects of the arc lamp and the spectrophotometer light source. Second, and perhaps more importantly, azoTAB in the *cis* form has a small but non-negligible absorbance at the excitation wavelength of YOYO-3, supplied predominantly as the 577-nm and 579-nm mercury lines by the fluorescence microscope. For example, even with a relatively low absorption coefficient of $0.013\ mM^{-1}cm^{-1}$ at 577 nm (background corrected) [33], the excitation light, which was highly focused through the microscope objective lens, was observed to result in a driving force for *cis*-to-*trans* isomerization sufficient to negate the *trans*-to-*cis* isomerization driven by relatively diffuse light from a

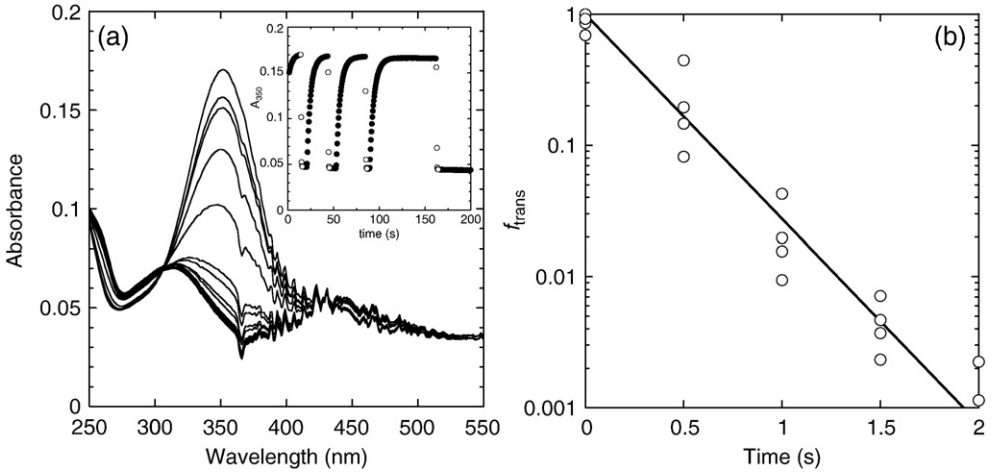

Fig. 4. Photoisomerization kinetics of a 700 μM azoTAB surfactant solution in a 0.1 mm cell. (a) Representative absorbance spectra during the course of isomerization. Inset: the absorbance at 350 nm as a function of time upon switching on and off the exposure to 365-nm light from the mercury arc lamp. Open symbols correspond to the displayed spectra. (b) Fitting of the *trans*-to-*cis* photoisomerization to first-order kinetics, with f_{trans} representing the fraction of surfactant remaining in the *trans* isomeric state upon exposure to 365-nm light.

200-W mercury arc lamp, expected to occur at a rate of $k \sim 1.6\ s^{-1}$ ($=0.4\ s^{-1} \times \varepsilon^{365}_{azoTAB}/\varepsilon^{365}_{C4AzoOC2E2}$). Indeed, this observation prompted the move to a 500-W bulb for all measurements in this work.

Thus, the conversion of azoTAB to the *trans* form driving DNA compaction would result from a combination of 435.8-nm light from the mercury arc lamp (near the maximum of the *cis* absorption band) and 577/579-nm light from the fluorescence microscope (at the tail of the *cis* band). Thus, the net *cis*-to-*trans* isomerization rate can be estimated as *ca.* $0.6 + 1.6 = 2.2\ s^{-1}$, equating to a half-life of ~0.3 s. Due to the fact that freely-diffusing DNA molecules in the elongated state would be expected to display a range of lengths projected into the focal plane in Fig. 3, a lag phase associated with this half-life, if present, cannot be detected. However, based on the time required to complete DNA compaction (~0.7 s), the rate of the DNA conformation transition once compaction is initiated by isomerization of sufficient azoTAB (within about ~0.3 s, based on an effective *r*-ratio of 125) would not be expected to be limited by the rate of surfactant isomerization. Indeed, no measurable difference in the net DNA condensation times was observed with utilization of the arc lamp ($k \sim 2.2\ s^{-1}$) or simply allowing the microscope excitation to convert the surfactant ($k \sim 1.6\ s^{-1}$, $t_{1/2} \sim 0.4$ s), indicating that absorbance at 577/579 nm was sufficient to induce isomerization fast enough so as to not limit DNA compaction. Of course this "microscope" *cis*-to-*trans* rate of $\sim 1.6\ s^{-1}$ also needs to be accounted for when considering the rate at which the arc lamp can induce a *trans*-to-*cis* isomerization within the microscope. Thus, the value of $3.5\ s^{-1}$ measured in the spectrophotometer in Fig. 4 would need to be reduced by $\sim 1.6\ s^{-1}$ to account for this effect, resulting in an effective rate of $\sim 1.9\ s^{-1}$, or a half-life of ~0.35 s, still below the time required for DNA expansion.

Nevertheless, to test the assumptions made above used to estimate the net *cis*-to-*trans* isomerization rate, control experiments were performed in which DNA compaction occurred independent of surfactant photoisomerization. As shown in Fig. 5, DNA compaction could be induced by carefully placing a 10-μL drop of a concentrated (1.25 mM) surfactant solution in a region adjacent to that being observed, as has been previously shown for mixtures of DNA with the surfactant CTAB [3]. In this manner, diffusion of surfactant molecules from the concentrated drop to nearby DNA molecules results in an increase in the local surfactant concentration around the DNA molecules sufficient to induce condensation. As seen in Fig. 5, this technique leads to condensation of T4-DNA within ~1 s (i.e., 166 kbp/s), similar to the rates of photo-induced condensation in Fig. 3 (240 kbp/s) despite the fact that in Fig. 5 the DNA molecule is initially in a slightly stretched conformation (i.e., end-to-end distances ~12 μm), likely due the convection associated with drop placement. Based on a root mean square displacement of the diffusing surfactant molecules ($\sqrt{6Dt}$, or 55 μm within a time *t* of 1 s for a nominal value of $D = 5 \times 10^{-6}\ cm^2/s$ for the surfactant diffusivity [41]), the local increase in surfactant concentration to compacting values is expected to occur over a relatively short time frame. Hence, the kinetics observed in Fig. 5 would be expected to be controlled by the inherent rate of DNA packing upon condensation, and not surfactant delivery.

The relatively fast photoisomerization rates obtained in Fig. 4, combined with the fact that similar compaction rates are obtained independent of photoisomerization in Figs. 3 and 5, support the assertion that the rates of photo-induced DNA conformational changes in Fig. 3 are not limited by surfactant isomerization. Instead, the coupled processes of surfactant binding/dissociation plus rearrangement of the DNA macromolecule appear to be rate limiting. The rates of surfactant association/dissociation with DNA would be expected to be similar to monomer-micelle exchange rates in pure surfactant solutions, which generally occur with microsecond time scales [42]. Moreover, surfactant diffusion to (or from) DNA molecules would be relatively rapid, as discussed above. Thus, the rates observed in Fig. 3 appear to be the true inherent rates of DNA conformational changes, and not limited by surfactant processes.

The ability to visualize DNA conformational changes triggered with light illumination, again without flow or mixing, also allows investigation of the mechanism of the compaction process in greater detail, as shown in Fig. 6. Upon initiating compaction with visible light from the UV-adapted state, many of the molecules were observed to contain bright spots at one or both ends of the DNA molecule, corresponding to regions with a high density of genetic material. This suggests that compaction is initiated at the ends of the molecule, subsequently proceeding towards the middle of the DNA chain. A similar mode of condensation was observed from elongated DNA stretched under flow [24,36,38]. Furthermore, Monte Carlo [27], Brownian Dynamics [26], and Molecular Dynamics [28] simulations of polymer collapse have all revealed the importance of the polymer ends as starting points for chain collapse. The time required for

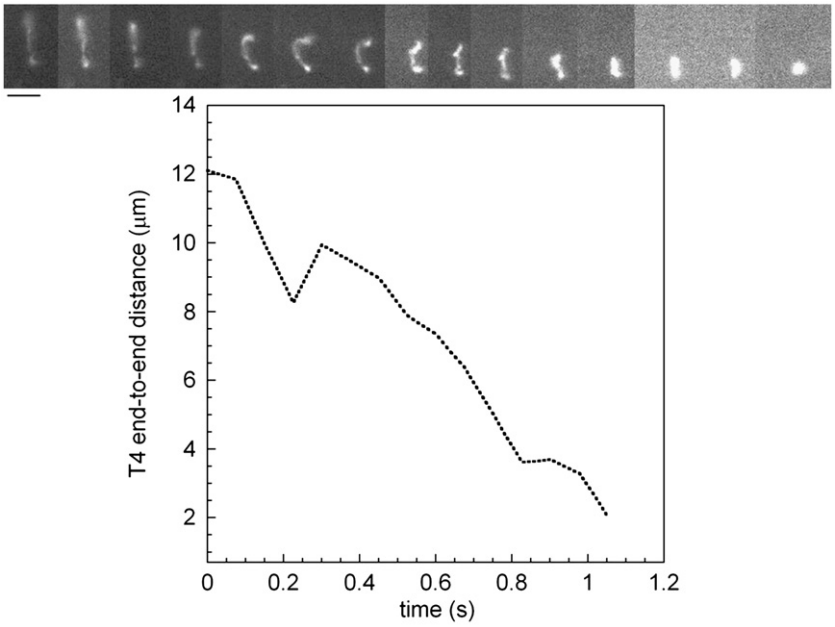

Fig. 5. Observation of T4-DNA compaction as surfactant diffuses from a concentrated drop placed adjacent to the DNA molecule. Scale bar = 5 μm.

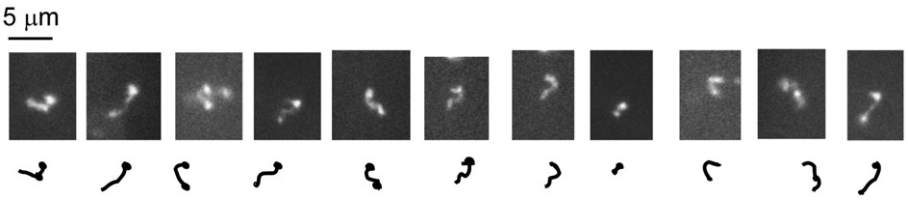

Fig. 6. Microscope images of representative DNA molecules taken during the compaction process, showing nucleation points located generally at the ends of the molecule.

compaction to occur is then linked to the time needed for the ends to "consume" the entire molecule [27]. This rate of consumption (expressed in units of kbp/s) would then be expected to be independent of DNA length (as opposed to the units of μm/s).

Thus, strictly speaking, the condensation rates reported upon either light illumination (240 kbp/s in Fig. 3) or rapid mixing (166 kbp/s in Fig. 5) should be divided by a factor of two to account for compaction initiating at both ends of the molecule. Interestingly, this would result in compaction rates similar to the reported maximum rate achieved upon addition of histones as the shear rate approaches zero in a flow cell, where DNA condenses from a single end at 103 kbp/s. This suggests that rates on the order of 100 kbp/s may be the limit for DNA packaging into condensed particles for both the photo-induced and shear-cell techniques. It should be noted, however, that bright spots were not always located at the ends of DNA molecules, although spots initially observed in the middle of DNA chains occurred much less frequently.

3.2. Fluorescence of ethidium bromide

To gain further insight into photo-initiated DNA expansion and compaction processes, ethidium bromide displacement studies were employed. Ethidium bromide exhibits a dramatic increase in fluorescence upon intercalation between DNA base pairs [43,44], a result of the probe becoming isolated from the solvent and, thereby, constrained from relaxation by donating a proton to the solvent. As a result, DNA condensation has been tracked by a decrease in ethidium bromide fluorescence upon the addition of a cationic species such as porphyrins [43], cationic liposomes [45], or the cationic surfactants cetyltrimethylammonium bromide, dodecyltrimethylammonium bromide, or tetradecyltrimethylammonium bromide [46–48]. Quenching of the dye has been linked to two possible mechanisms: displacement

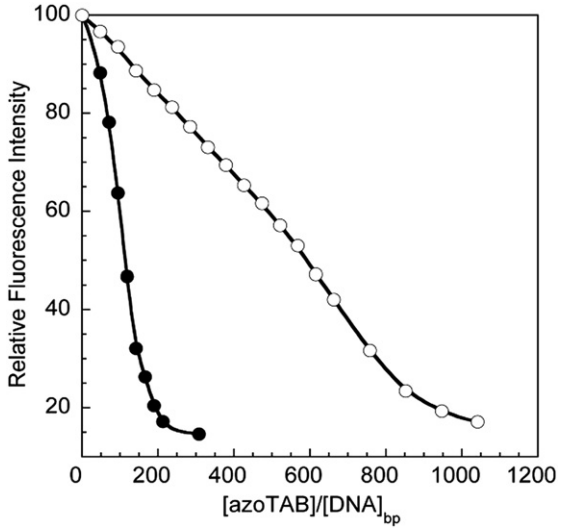

Fig. 7. Normalized fluorescence intensity of ethidium bromide as a function of the surfactant-to-DNA base pair ratio. Closed circles represent data taken with addition of *trans* surfactant, while open symbols represents spectra taken after addition of *cis* surfactant. [HT-DNA] = 0.6 μM, [EB] = 0.3 μM, λ^{ex} = 535 nm, λ^{em} = 595 nm.

of the fluorophore with the cationic condensation agent due to competition for electrostatic binding sites on DNA, and/or proton transfer with the solvent [49]. Moreover, a decrease in DNA flexibility upon condensation can shift the binding equilibrium of ethidium bromide towards the solution phase [50].

The addition of azoTAB surfactant to a solution of DNA complexed with ethidium bromide results in a decrease in the fluorescence of the probe, as shown in Fig. 7. A similar addition of surfactant to a solution free of DNA as a control experiment did not result in a decrease in fluorescence emission (results not shown). The concentration of DNA used was identical to that in the microscopic observations above. With the addition of the *trans* form of the surfactant, the fluorescence intensity of ethidium bromide rapidly decreases until an *r*-ratio of 200 is reached, upon which point the fluorescence remains at a constant 10% of the initial intensity. From Fig. 1, this *r*-ratio corresponds to the point where all DNA molecules are condensed. Similarly, addition of the *cis* form of the surfactant results in a maximum decrease in fluorescence at $r = 900$, again near the point where complete condensation is observed in Fig. 1. Thus, the relatively-hydrophilic *cis* form of the surfactant has a lower binding affinity towards DNA compared to the relatively-hydrophobic *trans* form, consistent with the observations above. Perhaps most telling is that both curves in Fig. 7 display a clear inflection point, a classic indication of the onset of cooperative hydrophobic binding between surfactant molecules [51]. Interestingly, these inflection points at $r \sim 150$ and $r \sim 600$ for *trans* and *cis* azoTAB, respectively, coincide with regions where the measured end-to-end distances in Fig. 1 rapidly decrease (i.e., where approximately 50% of DNA molecules are condensed).

While the mechanism of binding of azoTAB to DNA (intercalation and/or surface binding) can not be conclusively determined from these studies, the indication of a cooperative transition in Fig. 7 argues against intercalation as the only mode of surfactant binding, as intercalation would be expected to prevent cooperative surfactant-surfactant interactions. Furthermore, even though the non-planar *cis* form of the surfactant is not expected to be readily intercalated, DNA condensation is still observed under UV light, albeit at approximately 3–4 times higher surfactant concentrations than the planar *trans* isomer. Note that under UV-light over 90% of the surfactant molecules are converted to the *cis* isomer both in the absence [33] and in the presence [2] of DNA, hence, the small residual concentration of *trans* isomers would be insufficient to condense DNA alone based on Fig. 1. Similarly, significant π–π stacking interactions between azoTAB surfactant tails and cooperative surfactant binding to DNA was previously observed just prior to DNA condensation [2], further supporting surface binding as the primary mode of azoTAB interaction with DNA.

4. Conclusions

This study has demonstrated that DNA compaction can be reversibly and directly controlled with simple light illumination through the use of photoresponsive surfactants. The addition of azoTAB surfactant to a T4-DNA solution under visible light, where the surfactant primarily exists as the *trans*, relatively-hydrophobic isomer, causes DNA to adopt a compacted conformation. Exposure to UV light causes the compacted DNA to re-expand and recover the extended-

coil conformation, a result of photoisomerization of the surfactant to the relatively-hydrophilic *cis* form. This process can be photo-reversibly controlled virtually indefinitely without resulting in strand separation or photocleavage of the DNA. Kinetics of the photo-induced compaction and expansion processes are both estimated to occur at rates of about 9 μm/s or 240 kbp/s and thought to be limited by the intrinsic processes of the DNA molecule (as opposed to surfactant limited). Fluorescent images of DNA molecules undergoing compaction show the appearance of probable nucleation sites at the ends of the macromolecule, where compaction appears to be initiated. The fluorescence quenching of ethidium bromide upon surfactant addition reveals that both the *cis* and the *trans* forms of the azoTAB surfactant bind to DNA in a cooperative manner, ultimately inducing compaction of the molecule. The binding affinity of the *cis* form of the surfactant is, however, much lower than the *trans* conformer, thereby allowing for compaction and expansion of DNA to be rapidly triggered with light illumination.

Acknowledgements

This work was supported in part by the U.S. National Science Foundation under Grant Nos. 0829209 and 0508535. We also wish to thank Jing Zhang for synthesizing the surfactant.

References

[1] M.E. Cerritelli, N. Cheng, A.H. Rosenberg, C.E. McPherson, F.P. Booy, S.A.C., Encapsidated conformation of bacteriophage T7 DNA, Cell (1997) 271–280.
[2] A.-L.M. Le Ny, C.T. Lee Jr., Photoreversible DNA condensation using light-responsive surfactants, Journal of the American Chemical Society (2006) 6400–6408.
[3] S.M. Mel'nikov, V.G. Sergeyev, K. Yoshikawa, Discrete coil-globule transition of large DNA induced by cationic surfactant, Journal of the American Chemical Society (1995) 2401–2408.
[4] M.G. Miguel, A.A.C.C. Pais, R.S. Dias, C. Leal, M. Rosa, B. Lindman, DNA-cationic amphiphile interactions, Colloids and Surfaces. A, Physicochemical and Engineering Aspects (2003) 43–55.
[5] S.Z. Bathaie, A.A. Moosavi-Movahedi, A.A. Saboury, Energetic and binding properties of DNA upon interaction with dodecyl trimethylammonium bromide, Nucleic Acids Research 4 (1999) 1001–1005.
[6] S. Bhattacharya, S.S. Mandal, Interaction of surfactants with DNA. Role of hydrophobicity and surface charge on intercalation and DNA melting, Biochimica et Biophysica Acta (1997) 29–44.
[7] P.L. Felgner, T. Gadek, M. Holm, R. Roman, H. Chan, M. Wenz, J. Northrop, G. Ringold, M. Danielson, Lipofection: a highly efficient, lipid-mediated DNA-transfection procedure, Proceedings of the National Academy of Sciences of the United States of America (1987) 7413–7417.
[8] R.I. Mahato, A. Rolland, E. Tomlinson, Cationic lipid-based gene delivery systems: pharmaceutical perspectives, Pharmaceutical Research 7 (1997) 853–859.
[9] Y. Murayama, M. Sano, Exchange of counterions in DNA condensation, Biopolymers (2005) 354–360.
[10] I.S. Blagbrough, D. Al-Hadithi, A.J. Geall, Cheno-, urso- and deoxycholic acid spermine conjugates: relative binding affinities for calf thymus DNA, Tetrahedron (2000) 3439–3447.
[11] V.A. Bloomfield, DNA condensation by multivalent cations, Biopolymers 3 (1997) 269–282.
[12] C. Bustamante, T.W. Housel, D.A. Beach, M.F. Maestre, Fluorescence microscopy of the dynamics of supercoiling, folding and condensation of bacterial chromosomes, induced by acridine orange, Journal of Biomolecular Structure & Dynamics 3 (1990) 643–655.
[13] S.V. Mikhailenko, V.G. Sergeyev, A.A. Zinchenko, M.O. Gallyamov, I.V. Yaminsky, K. Yoshikawa, Interplay between folding/unfolding and helix/coil transitions in giant DNA, Biomacromolecules (2000) 597–603.
[14] K.B. Roy, T. Anthony, A. Saxena, H.B. Bohidar, Ethanol-induced condensation of calf thymus DNA studied by laser light scattering, Journal of Chemical Physics B (1999) 5117–5121.
[15] C.C. Conwell, I.D. Vilfan, N.V. Hud, Controlling the size if nanoscale toroidal DNA condensates with static curvature and ionic strength, Proceedings of the National Academy of Sciences of the United States of America 16 (2003) 9296–9301.
[16] C.C. Conwell, N.V. Hud, Evidence that both kinetic and thermodynamic factors govern DNA toroid dimensions: effects of magnesium(II) on DNA condensation by hexammine cobalt(III), Biochemistry (2004) 5380–5387.
[17] A. Remy-Kristensen, J.-P. Clamme, C. Vuilleumier, G. Duportail, J.-G. Khury, Y. Mély, Role of endocytosis in the transfection of L929 fibroblasts by polyethylenimine/DNA complexes, Biochimica et Biophysica Acta 1 (2001) 21–32.
[18] Y. Xu, F.C. Szoka Jr., Mechanism of DNA release from cationic/DNA complexes used in cell transfection, Biochemistry (1996) 5616–5623.
[19] D. Lechardeur, G.L. Lukacs, Intracellular barriers to non-viral gene transfer, Current Gene Therapy (2002) 183–194.
[20] D.V. Schaffer, N.A. Fidelman, N. Dan, D.A. Lauffenburger, Vector unpacking as a potential barrier for receptor-mediated polyplex gene delivery, Biotechnology and Bioengineering (2000) 598–606.
[21] M.L. Read, K.H. Bremner, D. Oupicky, N.K. Green, P.F. Searle, L.W. Seymour, Vectors based on reducible polycations facilitate intracellular release of nucleic acid, The Journal of Gene Medicine (2003) 232–245.
[22] N. Makita, K. Yoshikawa, Proton concentration (pH) switches the higher-order structure of DNA in the presence of spermine, Biophysical Journal (2002) 43–53.
[23] K. Yoshikawa, Controlling the higher-order structure of giant DNA molecules, Advanced Drug Delivery Reviews (2001) 235–244.
[24] L.R. Brewer, M. Corzett, R. Balhorn, Protamine-induced condensation and decondensation of the same DNA molecule, Science (1999) 120–123.
[25] M.E. Hays, C.M. Jewell, D.M. Lynn, N.L. Abbott, Reversible condensation of DNA using a redox-active surfactant, Langmuir 10 (2007) 5609–5614.
[26] G.G. Pereira, D.R.M. Williams, Kinetic pathways for the collapse of semiflexibles polymers, The ANZIAM Journal (2004) C163–C173.
[27] B. Ostrovski, Y. Bar-Yam, Motion of polymer ends in homopolymer and heteropolymer collapse, Biophysical Journal 5 (1995) 1694–1698.
[28] M.J. Stevens, Simple DNA condensation, Biophysical Journal (2001) 130–139.
[29] A. Hamill, S.C. Wang, C.T. Lee Jr., Probing lysozyme conformation with light reveals a new folding intermediate, Biochemistry 46 (2005) 15139–15149.
[30] C.T. Lee Jr., K.A. Smith, T.A. Hatton, Photocontrol of protein folding: the interaction of photoresponsive surfactants with bovine serum albumine, Biochemistry 2 (2005) 524–536.
[31] S.-C. Wang, C.T. Lee Jr., Protein secondary structure controlled with light and photoresponsive surfactants, Journal of Physical Chemistry B 32 (2006) 16117–16123.
[32] T. Hayashita, T. Kurosawa, T. Miyata, K. Tanaka, M. Igawa, Effect of structural variation within cationic azo-surfactant upon photoresponsive function in aqueous solution, Colloid and Polymer Science (1994) 1611–1616.
[33] C.T. Lee Jr., K.A. Smith, T.A. Hatton, Photoreversible viscosity changes and gelation in mixtures of hydrophobically modified polyelectrolytes and photosensitive surfactants, Macromolecules (2004) 5397–5405.
[34] R.S. Dias, B. Lindman, M.G. Miguel, Compaction and decompaction of DNA in the presence of catanionic amphiphile mixtures, Journal of Chemical Physics B (2002) 12608–12612.
[35] S.M. Mel'nikov, V.G. Sergeyev, K. Yoshikawa, Transition of double stranded DNA chains between random coil and compact globule states induced by cooperative binding of cationic surfactant, Journal of the American Chemical Society (1995) 9951–9956.
[36] L. Brewer, M. Corzett, R. Balhorn, Condensation of DNA by spermatid basic nuclear proteins, Journal of Biological Chemistry 41 (2002) 38895–38900.
[37] B. Ladoux, J.-P. Quivy, P. Doyle, O. du Roure, G. Almouzni, J.-L. Viovy, Fast kinetics of chromatin assembly revealed by single-molecule videomicroscopy and scanning force microscopy, Proceedings of the National Academy of Sciences of the United States of America 26 (2000) 14251–14256.
[38] G. Wagner, A. Bancaud, J.-P. Quivy, C. Clapier, G. Almouzni, J.-L. Viovy, Conpaction kinetics on single DNAs: purified nucleosome reconstitution systems versus crude extract, Biophysic journal (2005) 3647–3659.
[39] T. Shang, K.A. Smith, T.A. Hatton, Photoresponsive surfactants exhibiting unusually large, reversible surface tension changes under varying illumination conditions, Langmuir (2003) 10764–10773.
[40] B.A. Cicciarelli, T.A. Hatton, K.A. Smith, Dynamic surface tension behavior in a photoresponsive surfactant system, Langmuir (2007) 4753–4764.
[41] J.K. Ferri, K.J. Stebe, Which surfactants reduce surface tension faster? A scaling argument for diffusion-controlled adsorption, Advances in Colloid and Interface Science (2000) 61–97.
[42] K.K. Fox, Determination of the monomer-micelle exchange frequency of a paramagnetic surfactant, Transactions of the Faraday Society (1971) 2802–2809.
[43] R.F. Pasternack, M. Caccam, B. Keogh, T.A. Stephenson, A.P. Williams, E.J. Gibbs, Long-range fluorescence quenching of ethidium ion by cationic porphyrins in the presence of DNA, Journal of the American Chemical Society (1991) 6835–6840.
[44] M. Tecle, M. Preuss, A.D. Miller, Kinetic study of DNA condensation by cationic peptides used in nonviral gene therapy: analogy of DNA condensation to protein folding, Biochemistry 35 (2003) 10343–10347.
[45] H. Gershon, R. Ghirlando, S.B. Guttman, A. Minsky, Mode of formation and structural features of DNA-cationic liposome complexes used for transfection, Biochemistry (1993) 7132–7151.
[46] V.A. Izumrudov, M.V. Zhiryakova, A.A. Goulko, Ethidium bromide as a promising probe for studying DNA interaction with cationic amphiphiles and stability of the resulting complexes, Langmuir (2002) 10348–10356.
[47] D.M. McLoughlin, J. O'brien, J.J. McManus, A.V. Gorelov, K.A. Dawson, A simple and effective separation and purification procedure for DNA fragments using Dodecyltrimethylammonium bromide, Bioseparation 5 (2000) 307–313.
[48] S.J. Eastman, C. Siegel, J. Tousignant, A.E. Smith, S.H. Cheng, R.K. Scheule, Biophysical characterization of cationic lipid: DNA complexes, Biochimica et Biophysica Acta. Biomembranes 1 (1997) 41–62.
[49] J.-B. LePecq, C. Paoletti, A fluorescent complex between ethidium bromide and nucleic acids. Physical-chemical characterization, Journal of Molecular Biology (1967) 87–106.
[50] A.J. Geall, I.S. Blagbrough, Rapis and sensitive ethidium bromide fluorescence quenching assay of polyamine conjugate-DNA interactions for the analysis of lipoplex formation in gene therapy, Journal of Pharmaceutical and Biomedical Analysis (2000) 849–859.
[51] K. Holmberg, B. Jönsson, B. Kronberg, B. Lindman, in: Wiley (Ed.), Surfactants and polymers in aqueous solution, 2003, p. 545.